

# Sodium in the Sun and in metal-poor stars<sup>\*</sup>

D. Baumüller, K. Butler, and T. Gehren

Institut für Astronomie und Astrophysik der Universität München, Scheinerstrasse 1, D-81679 München, Germany  
(butler@usm.uni-muenchen.de, gehren@usm.uni-muenchen.de)

Received 30 March 1998 / Accepted 8 July 1998

**Abstract.** Systematic effects in the statistical equilibrium of sodium in cool metal-poor stars are analyzed using full NLTE line formation. To determine the important influence of collision processes and of the atomic model, NLTE effects of neutral sodium are first evaluated in the solar photosphere where the statistical equilibrium of Na I can be followed by examination of a relatively large number of line transitions. In agreement with previous analyses it is found that even very simple atomic models are sufficient to describe the most important interactions. In the solar atmosphere the inner cores of the lines are most affected by deviations from LTE, but the corresponding abundance corrections due to NLTE populations are small. The influence of collisional interactions with electrons and hydrogen atoms is evaluated by comparison of the solar spectrum with very precise fits to the Na I line cores. The profile analysis depends sensitively on the appropriate choice of velocity amplitudes and its variation with depth. The resulting solar sodium abundance is obtained with small scatter,  $\log \varepsilon_{\text{Na},\odot} = 6.30 \pm 0.03$ .

In *metal-poor stars* NLTE effects are more pronounced since the statistical equilibrium is dominated by collisions in which at least the electronic component is substantially reduced. The resulting influence on the determination of Na abundances is in a direction opposite to that found previously for Al. Stars determined in LTE analyses to have a solar [Na/Fe] ratio reveal a lower [Na/Fe] when NLTE line formation is taken into account. As for aluminium, the extremely metal-poor and the hotter subdwarfs are affected most strongly by Na abundance corrections reaching  $-0.5$  dex for the D lines. The resulting Galactic evolution of the Na/Fe and Na/Mg ratios is not adequately described by current chemical evolution scenarios.

**Key words:** atomic processes – line: formation – Sun: abundances – Sun: photosphere – stars: abundances – Galaxy: evolution

## 1. Introduction

Similarly to the  $^{27}\text{Al}$  nucleus  $^{23}\text{Na}$  contains an extra neutron that makes its synthesis deviate from that of the  $\alpha$ -nuclei  $^{20}\text{Ne}$

Send offprint requests to: T. Gehren

<sup>\*</sup> Based on observations collected at the European Southern Observatory, La Silla, Chile, and at the German-Spanish Astronomical Center, Calar Alto, Spain

or  $^{24}\text{Mg}$ . Therefore the abundance ratio Na/Fe in metal-poor stars is a potential source of information concerning the early history of Galactic nucleosynthesis. From a stellar nucleosynthesis point of view it should possess very similar properties to those found in a recent analysis of the Al spectra in metal-poor stars (Baumüller & Gehren 1997, Paper II). The central question with respect to sodium is whether  $^{23}\text{Na}$  is synthesized as a *primary* or a *secondary* element. In the first case  $^{23}\text{Na}$  would be produced directly in the carbon burning process, and the production rate would be independent of the metal content of the preceding stellar generation. In the second process, where  $^{23}\text{Na}$  is produced by neutron or proton capture, the production rate would depend on the *neutron excess* which in turn would be determined by the pre-existing metal abundance. In the latter case  $^{23}\text{Na}$  would be expected to display an underabundance compared with iron in the most metal-poor stars.

Most previous abundance determinations of Na have been carried out under the assumption of local thermodynamic equilibrium (LTE). The corresponding results for metal-poor stars are similar to those for aluminium in that both element abundances show a few typical features.

- From solar-type stars the [Al/Fe] and [Na/Fe] abundance ratios tend to *increase* smoothly with decreasing [Fe/H], as determined by Edvardsson et al. (1993). As is evident in Fig. 1, the effect is small for sodium abundance ratios.
- Near [Fe/H] =  $-1$  the [Na/Fe] ratios start to *decrease* with decreasing [Fe/H]. Again this trend is not as clear as that for aluminium, and the minimum [Na/Fe] ratios approach 1/10 of the solar value. Some of the most metal-poor stars known today seem to tend to [Na/Fe] = 0 or even display [Na/Fe] ratios above 0 (e.g. Bessell & Norris 1984; McWilliam et al. 1995).
- Around [Fe/H] =  $-1$  there seems to be a hump in the [Na/Fe] ratio with a corresponding overabundance of sodium. At present it is not clear whether this is an artefact of the abundance analysis due to the selection of spectral lines.

Previous analyses of sodium in the *solar atmosphere* allowing for deviations from LTE (Athay & Canfield 1969; Gehren 1975; Caccin et al. 1980; 1993, Bruls et al. 1992; Takeda 1995; Mashonkina et al. 1993, 1998) seem to agree that the statistical equilibrium of sodium in the upper photosphere produces

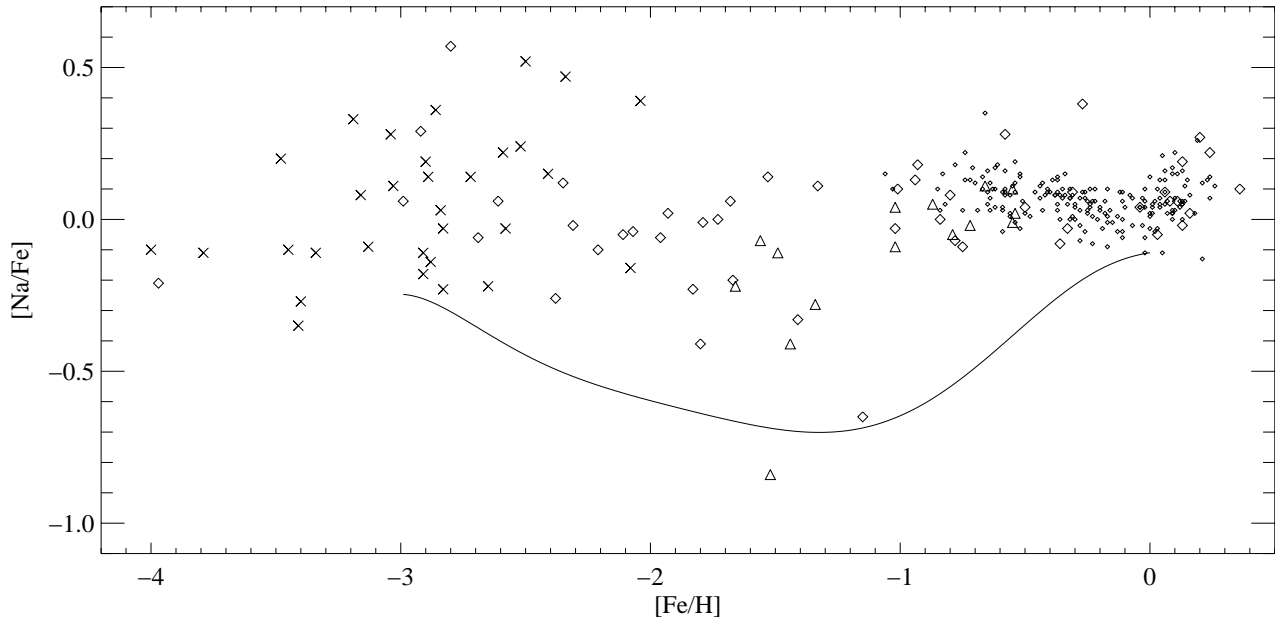


**Fig. 1.** Sodium abundances of metal-poor stars determined from LTE analyses of Peterson (1981,  $\triangle$ ), Gratton & Sneden (1987, 1988,  $\diamond$ ), McWilliam et al. (1995,  $\times$ ) and Edvardsson et al. (1993, dots). The curve represents the standard chemical evolution model calculated by Timmes et al. (1995)

small but non-negligible influences on the formation of the Na *line cores* that are seen in the D lines (with most contributions from chromospheric layers) but also in the subordinate doublets arising from the  $3p^2P^o$  terms at 5682/5688 Å ( $3p^2P^o - 4d^2D$ ), 6154/6160 Å ( $3p^2P^o - 5s^2S_{1/2}$ ), 8183/8194 Å ( $3p^2P^o - 3d^2D$ ), and at 1.14  $\mu\text{m}$  ( $3p^2P^o - 4s^2S_{1/2}$ ) in photospheric layers between  $\log \tau_{5000} \approx -1$  and  $-2$ . Whereas the choice of the *atmospheric* model has only a minor influence on the emerging line spectra since photoionization is unimportant, the *atomic* model must be carefully determined by comparison with the solar line cores. For the Sun we have excellent spectra covering a wide range of wavelengths, and all influences of model completeness such as the correct representation of the collisional interaction can be tested there and compared with previous investigations. Section 2 therefore contains a detailed discussion of the NLTE line formation that is the basis of our calculations. Section 3 presents the statistical equilibrium of Na I in the solar atmosphere, the reaction of the synthetic line profiles to variations of the atomic and atmospheric models, and the solar abundance of sodium.

NLTE effects that are small in the solar atmosphere are expected to be much more pronounced in metal-poor stars, where thermalization through collisional interaction is reduced substantially in its efficiency. The atomic model found to give a good representation of sodium in the solar photosphere is used in Sect. 4 to model the statistical equilibrium in metal-poor atmospheres. The level populations result in line profiles considerably different from those found for LTE. Accordingly, the Na/Fe and Na/Mg abundance ratios display a different pattern when plotted as a function of metal abundance. The consequences of the new abundance determinations are discussed with respect to

stellar nucleosynthesis and Galactic chemical evolution in the final section.

## 2. NLTE line formation

Line formation – whether in LTE or based on statistical equilibrium – is affected by both the atomic and atmospheric models. Moreover, the dependence of the resulting synthetic spectra on such model assumptions can be different in stars with a broad range in effective temperatures, surface gravities and metal abundances. It is therefore important to test the possible effects of model variations with respect to spectrum synthesis. In the two following subsections this will be described with statistical equilibrium calculations using the DETAIL code of Giddings (1981; cf. Butler & Giddings 1985) which is based on the method of complete linearization described by Auer & Hearsley (1976).

In contrast to photoionization-dominated atoms the statistical equilibrium of Na in the solar atmosphere does *not* depend very much on the *size* of the atomic model. Since Na I is a simple one-electron system it is, however, easy to calculate a relatively complete neutral model atom with 45 terms describing the complete doublet system with principal quantum numbers  $n \leq 11$  and angular quantum numbers  $l \leq n-1$ . Only part of that model is shown in Fig. 2. The model is completed with the  $\text{Na}^+$  ground state. Fine structure splitting is neglected with the exception of  $3p^2P^o_{1/2}$  and  $3p^2P^o_{3/2}$ . Energy levels are taken from Martin & Zalubas (1981) if available. For levels with  $l > 3$  hydrogenic approximations are used.

The probabilities for radiative transitions between levels with  $n \leq 10$  and  $l \leq 3$  as well as the photoionization cross-sections for these levels were taken from unpublished work of

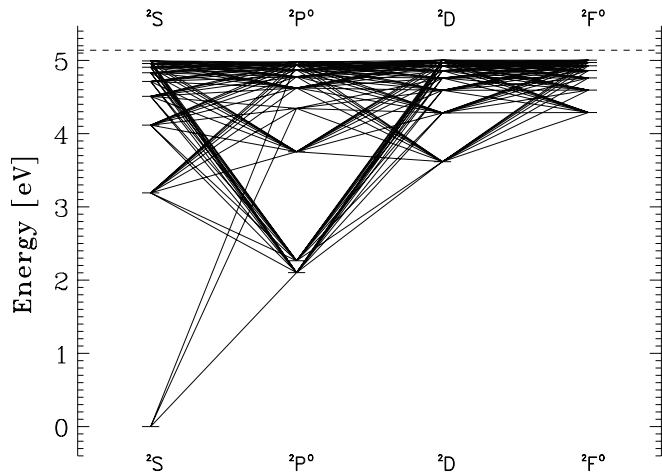


**Fig. 2.** Part of energy level diagram of neutral sodium displaying linearized radiative transitions; therefore only terms with  $l \leq 3$  are plotted

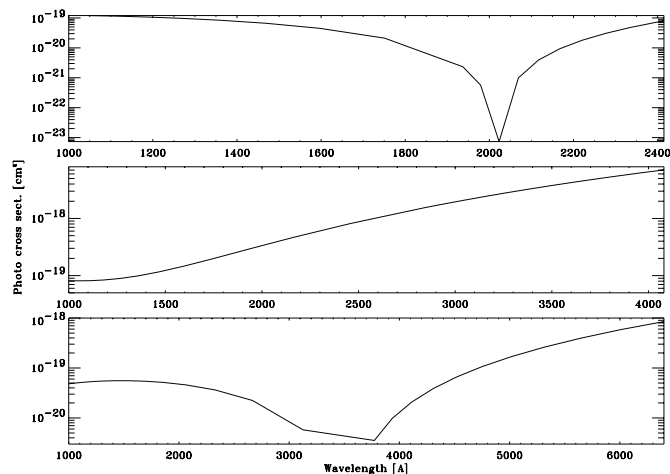


**Fig. 3.** Photoionization cross-sections (Butler 1993) of  $3s^2S_{1/2}$  (top),  $3p^2P^\circ$  (middle) and  $4s^2S_{1/2}$  (bottom)

K. Taylor for the *Opacity Project*. The data are available via TOPBASE (Cunto et al. 1993). The most important results are reproduced in Fig. 3 which indicates the differences between the  $^2S$  and the  $^2P^\circ$  systems. All other transition probabilities are assumed to follow the hydrogenic approximation; the data are taken from Green et al. (1957). The  $b$ - $b$  radiative transitions with  $l \leq 3$  are linearized (cf. Fig. 2), mostly represented by Doppler profiles. The resonance lines are treated using Voigt profiles fully accounting for radiative and van der Waals damping. The  $b$ - $f$  radiative transitions from the 5 lowest energy levels up to  $4p^2P^\circ$  are also linearized.

In the atmospheres of cool stars collisions with both electrons and neutral hydrogen atoms can thermalize the statistical equilibrium significantly. In metal-poor stellar atmospheres electron collisions are of reduced efficiency due to the low abundances of electron-donating metals, and here hydrogen collisions are the main thermalizing process. It is therefore very important to know the ratio of the respective collision rates with

sufficient reliability. At present this can be obtained neither from theory nor from experiment.

The collisions with electrons are approximated by the simple formula of van Regemorter (1962). According to more recent estimates of Sampson & Zhang (1992) this approximation is valid for special cases only; at least for transitions of the type  $\Delta n = 0$  van Regemorter's formula apparently leads to quite reasonable results and, fortunately, transitions of this type are most important for the statistical equilibrium of sodium. Thus the use of this approximation seems to be appropriate, particularly because the sodium populations are not very sensitive to the exact formulation of the collisional interaction.

The approximations for collisions with neutral hydrogen are even more rudimentary and are based on the formula of Drawin (1968) which was first applied by Gehren (1975). It is most often used in a form due to Steenbeck & Holweger (1984) although the validity of this latter formula cannot be judged. It contains a factor  $m_A/m_H$ , the ratio of atomic and hydrogen mass, the meaning of which is not clear to us because the original formula was published for atoms of the same type. Another reformulation by Lambert (1993) does not really solve the discrepancy since it only extends the cross-section to lower threshold energies. The basic result of the experimental and theoretical data available for the Na I  $3s^2S_{1/2}$ - $3p^2P_{1/2,3/2}^\circ$  transitions is that Drawin's formula yields cross-sections that are a factor between 10 and 100 too large. Whereas our present calculations do not support such a discrepancy for the Na I resonance lines, we note that all our models that are intended to reproduce highly excited Al I and Mg I lines (see Baumüller & Gehren 1996, 1997; Zhao et al. 1998) seem to require substantially reduced hydrogen collision rates when Drawin's formula is used. This is in rough accordance with calculations of Kaulakys (1985, 1986) for inelastic collisions between neutral and Rydberg atoms. The pragmatic solution to this problem is the usual application of a scaling factor for hydrogen collisions,  $S_H$ . For aluminium and magnesium it was found necessary to discriminate between lines of low and high excitation energy, where in both atoms the highly excited transitions required very small scaling factors  $S_H \approx 0.001 \dots 0.002$ , and the lines below 5 or 6 eV fit the solar spectrum much better with larger  $S_H$ , between 0.1 and 1.0 (or even more, cf. Paper I, and Zhao et al. 1998).

In the case of Na we consider  $S_H$  to be a free parameter to be fixed by solar and, if possible, stellar line spectra. All other atomic data are approximated as described in Baumüller & Gehren (1996)

### 2.1. Model atmospheres

Our statistical equilibrium calculations are based on horizontally homogeneous LTE model atmospheres in hydrostatic equilibrium (cf. Papers I and II). We account for metallic UV line absorption using Kurucz' (1992) opacity distribution functions interpolated for the proper mix of abundances. The solar abundances are adopted from Holweger (1979) with minor modifications for carbon (Stürenberg & Holweger 1990). For iron we use the meteoritic value of 7.51, a value we confirm from a

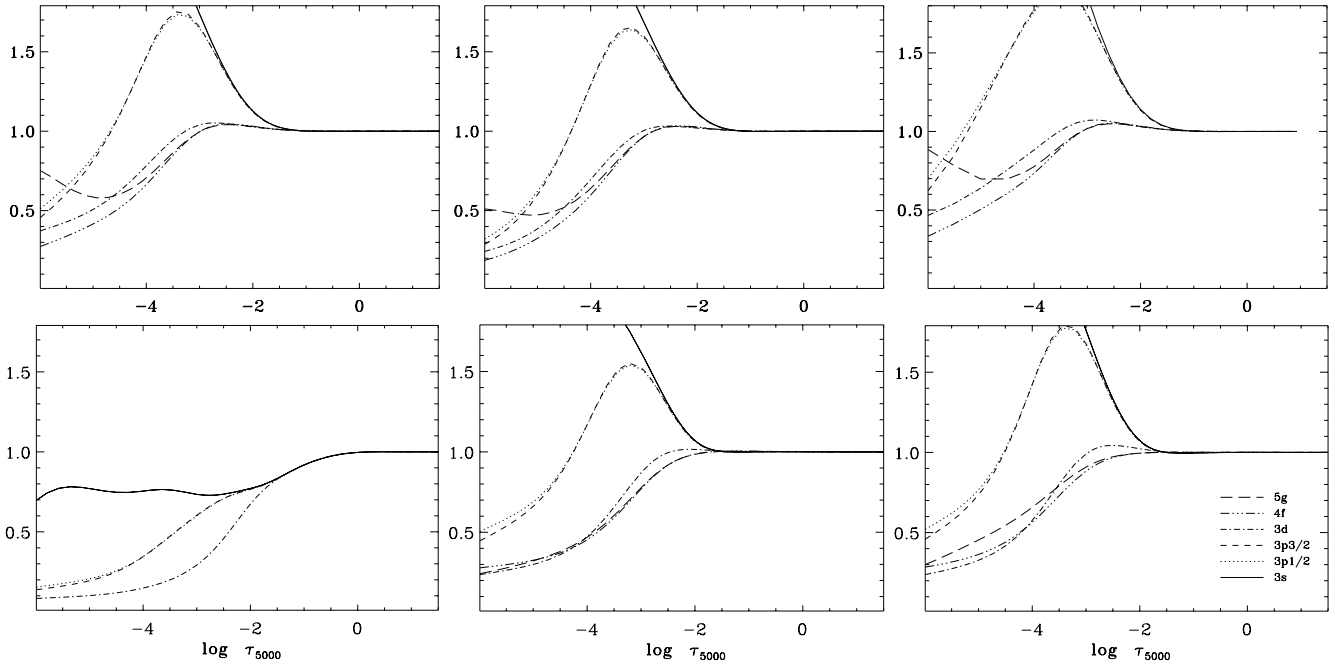


**Fig. 4.** Departure coefficients  $n_k/n_k^{\text{LTE}}$  of Na I in the solar atmosphere. **Top** (left): standard model including ODF opacities, (middle): standard model without ODF opacities, (right): Holweger-Müller (1974) model including ODF opacities. **Bottom** (left to right): Atomic models with increasing number of bound levels (4, 6, and 9)

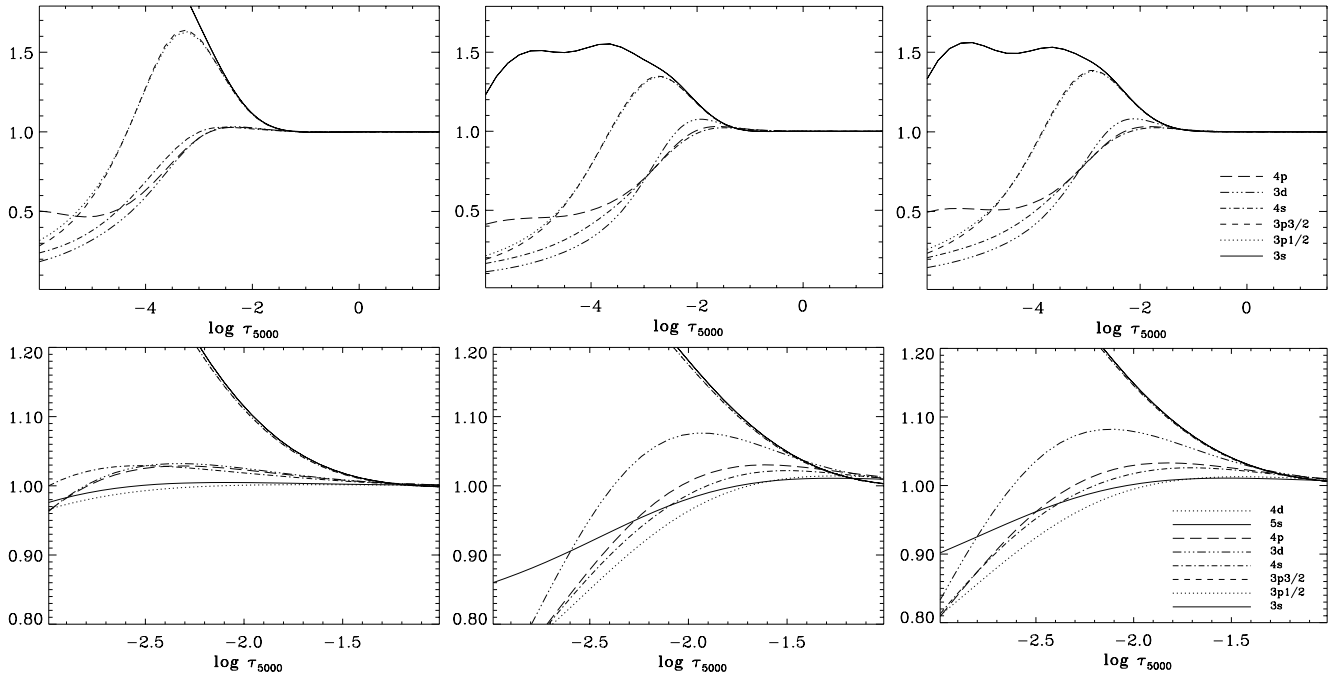


**Fig. 5.** Departure coefficients of Na I in the solar atmosphere. (Left): excluding hydrogen collisions ( $S_{\text{H}} = 0$ ); (middle): including hydrogen collisions ( $S_{\text{H}} = 0.5$ ); (right): no hydrogen collisions, but electron collision rates increased by a factor 2. The bottom row displays the enlarged region between optical depths  $\tau_c = 10^{-3}$  and  $10^{-1}$  from where most of the flux profiles emerge

corresponding Fe abundance analysis using the ODF-blanketed solar model atmosphere.

As in our analysis of the solar aluminium lines no attempt has been undertaken to model the solar *chromospheric* temperature rise. All previous work on Na suggests that this has an impor-

tant influence on the very cores of the D lines. However, the D line source functions depend on the *ratio* of the corresponding population densities, and this does not seem to depend much on the temperature stratification. The resonance line cores are, however, influenced by non-thermal and depth-dependent ve-

locity fields that are *not* part of our solar and stellar models. To account for this, a large increase of the microturbulence in the lower solar chromosphere would have to be used as proposed e.g. by Gehren (1975). In our present analysis we replace the chromospheric microturbulence by a single number that is determined from the D line core fit being aware that this choice does *not* affect the other line parameters (except macroturbulence). For all other lines the microturbulence has been allowed to increase with the depth of line-forming layers, with the most probable non-thermal velocities for flux profiles increasing from 0.7 to 1.0 km s<sup>-1</sup>, and 1.3 km s<sup>-1</sup> for intensity profiles at the solar center. In view of the application to *stellar* line formation this is not satisfactory; therefore a less detailed analysis of the solar Na I flux line spectrum has used a single microturbulence velocity of  $\xi = 0.8$  km s<sup>-1</sup>. Its result is taken as reference for the metal-poor stars.

For the investigation of metal-poor objects the same type of model is used to calculate stellar atmospheres with different parameters. The stellar parameters are taken from the new analyses of Fuhrmann et al. (1997, and private communication), or rederived from the work of Axer et al. (1994) on the basis of the new HIPPARCOS parallaxes (1997). Microturbulence is assumed constant with depth in all these stars.

Background opacities that determine the radiation field of the bound-free transitions through metal line absorption in the UV are obtained using the opacity distribution functions of Kurucz (1992). Sodium has only a few lines in the UV. Furthermore, the photoionization cross-sections of the lower levels are small. Thus the statistical equilibrium is hardly affected by the ultraviolet radiation field as is shown in the top row of Fig. 4. The semi-empirical solar model of Holweger & Müller (1974) has been used as an alternative to our standard model. Though the departure coefficients in Fig. 4 look slightly different, the profiles of the lines do not differ significantly, since most lines emerge from optical depths  $\tau_c \geq 10^{-3}$  where changes are small. We note, however, that the use of the Holweger & Müller model implies substantial changes in the determination of the damping constants.

## 2.2. Atomic models

Though the results obtained for the solar atmosphere do not depend much on the size of the atomic model it is useful to analyze the response of the line profiles to the different approximations. Most interesting is the simple description of the atomic model structure that allows the important features of the statistical equilibrium in the Sun to be recovered with only 6 levels. This is demonstrated in the bottom row of Fig. 4 where the departure coefficients for atomic models of increasing complexity are shown.

However, the fine details in profile synthesis require that the representation of the excited levels be sufficiently complete, as described above. Additionally, it is necessary to investigate the influence of collisions on the line formation. Whereas electron collisions dominate at optical depths  $\tau_c \geq 10^{-1}$  the hydrogen collisions are generally more important in the upper photo-

sphere. Their influence has been studied by varying the scaling factor  $S_H$  between 0 and 5. The results for these two limiting values are reproduced in Fig. 5, and it is evident how thermalization affects the low level departure coefficients in the outer layers where the hydrogen collision rates are increased. The best fit to the observed line profiles will be determined in the next section.

## 3. Sodium in the solar photosphere

Na I departure coefficients  $b_k = n_k/n_k^{\text{LTE}}$  in the solar atmosphere are best characterized by the overpopulation of the ground state  $3s^2S_{1/2}$  and the first excited states  $3p^2P^o$  in higher atmospheric layers beyond  $\log \tau_c = -1.5$ . The departure coefficients diverge outside  $\log \tau_c \approx -2 \dots -3$ . The excited states follow the overpopulation to a lesser extent and only in deeper atmospheric layers; therefore the strongest deviations from LTE in the photosphere should be expected for the subordinate lines arising from the  $3p^2P^o$  states near 2.1 eV. The origin of the overpopulation of the two lowest levels is the *photon suction* process described in detail by Bruls et al. (1992). It is triggered by photon losses in the lines. The strong resonance lines are optically thick over a wide depth range. Due to the reduced efficiency of collisions in the higher atmospheric layers the collisional de-excitation rates are small and the photons can be scattered over longer distances without being thermalized. Besides the resonance lines there are other strong lines for transitions with  $\Delta n = 0$ . A cascade of transitions via  $3s-3p-3d-4f$  connects the lowest levels with the continuum. Photon losses in these infrared lines result in a downward flow of electrons producing a statistical equilibrium with a relative overpopulation of the lower levels as demonstrated nicely in the bottom row of Fig. 4. It can be shown that these transitions dominate the statistical equilibrium and that due to this fact the collisional interactions between other transitions are less important.

The rates of the allowed electronic collisions are proportional to the  $f$  value. This is the reason why the transitions between only a few levels dominate, and an increase of the collision rates including hydrogen collisions scaled by  $S_H \approx 0.5$  (see Fig. 5) or even 1.0 does not change the populations very much. Only the very line *cores* of the NLTE profiles are sensitive to changes in  $S_H$ , and their migration towards LTE would require substantial enhancements of the hydrogen collision rates with scaling factors well above 10.

### 3.1. Line profiles and atomic model iteration

Our approach is similar to that of Baumüller & Gehren (1996). The present analysis of the solar Na spectrum is not intended to demonstrate spectacular changes in our understanding of NLTE line formation; it is rather intended as a replacement for non-existing laboratory experiments, to fix a parameter combination of model atmospheres and model atoms. Laboratory measurements are thus replaced by the observed solar line profiles taken from the Kitt Peak Solar Flux Atlas (Kurucz et al. 1984), and are compared with synthetic line profiles calculated from the

**Table 1.** Na I line data. Results (a) refer to NLTE abundances obtained with a constant  $\xi = 0.9 \text{ km s}^{-1}$ ,  $\Xi_{\text{rt}} = 3.2 \text{ km s}^{-1}$ . (b) denotes best fit results with parameters described in the last two columns

$\lambda$ [Å]	Transition	$\log gf$	$\log C_6$	$\log C_4$	$\log \varepsilon_{\text{Na}, \odot}$		$\xi$	$\Xi_{\text{rt}}$ [km s <sup>-1</sup> ]
					NLTE(a)	NLTE(b)		
5889.95	$3s^2S_{1/2} - 3p^2P_{1/2}^o$	0.11	-31.66	-16.41	6.32	6.32	1.5	4.5
5895.92	$3s^2S_{1/2} - 3p^2P_{3/2}^o$	-0.19	-31.66	-16.41	6.30	6.30	1.5	4.5
8183.26	$3p^2P_{1/2}^o - 3d^2D_{3/2}$	0.24	-31.01	-14.52	6.32	6.33	1.0	2.8
8194.80	$3p^2P_{3/2}^o - 3d^2D_{5/2}$	0.53	-31.01	-14.52	6.30	6.28	0.8	2.2
5682.64	$3p^2P_{1/2}^o - 4d^2D_{3/2}$	-0.71	-30.42	-12.74	6.29	6.30	0.8	3.0
5688.20	$3p^2P_{3/2}^o - 4d^2D_{5/2}$	-0.40	-30.42	-12.74	6.32	6.31	0.8	3.0
4982.83	$3p^2P_{3/2}^o - 5d^2D_{5/2}$	-0.95	-30.01	-11.85	6.31	6.30	1.0	3.2
4668.57	$3p^2P_{3/2}^o - 6d^2D_{5/2}$	-1.30	-29.69	-11.20	6.23	6.23	1.0	3.6
4497.68	$3p^2P_{3/2}^o - 7d^2D_{5/2}$	-1.56	-29.42	-9.67	6.27	6.22	1.0	4.2
6154.23	$3p^2P_{1/2}^o - 5s^2S_{1/2}$	-1.55	-30.59	-14.63	6.26	6.28	0.8	3.7
6160.75	$3p^2P_{3/2}^o - 5s^2S_{1/2}$	-1.26	-30.59	-14.63	6.26	6.30	0.8	3.5
5148.84	$3p^2P_{1/2}^o - 6s^2S_{1/2}$	-2.07	-30.14	-13.95	6.25	6.26	1.0	3.4
4751.82	$3p^2P_{1/2}^o - 7s^2S_{1/2}$	-2.10	-29.79	-13.41	6.27	6.25	1.0	3.5
10746.44	$4s^2S_{1/2} - 5p^2P_{3/2}^o$	-1.29	-30.40	-13.98	6.19	6.33	1.0	4.0
10834.87	$3d^2D - 6f^2F^o$	-0.25	-29.71	-9.52	6.27	6.25	1.0	3.2

level populations according to the NLTE departure coefficients obtained for a large number of different input parameters. The corresponding line data for the final fit are given in Table 1.

In accordance with Paper I, the synthetic profiles are convolved with a combination of a flux rotation profile of  $v_{\text{rot}, \odot} = 1.7 \text{ km s}^{-1}$  and a radial-tangential macroturbulence  $\Xi_{\text{rt}}$  which was found to vary for lines of different mean depth of formation between 2.2 and 4.5  $\text{km s}^{-1}$ . A few results are immediately evident from the solar Na lines reproduced in Fig. 6,

- the LTE profiles are generally too weak in the line cores, even in the subordinate lines,
- this defect of the LTE profiles exists for both the semi-empirical model of Holweger & Müller (1974) and our theoretical line-blanketed solar atmosphere. However, due to the flatter temperature gradient the *empirical model* produces even shallower profiles,
- only the NLTE profiles converge towards an acceptable fit of the observed line cores.

Our analysis of the solar line flux profiles is based on the adjustment of the input parameters in the same way as the automatic profile fits published by Takeda (1995). This includes the following data,

1. The appropriate selection of NLTE atomic models with particular emphasis on the collisional interaction with neutral hydrogen atoms. Fig. 5 suggests that in the Sun the influence of electron and hydrogen collisions derived from the corresponding approximations is very similar, at least inside  $\log \tau_c = -3$ . Therefore it is adequate to adjust only one of the two interaction rates; our decision is to accept the formula for electron collisions given by van Regemorter (1962), and modify only the uncertain formula for hydrogen collisions with the scaling factor  $S_{\text{H}}$ . The corresponding NLTE test calculations cover a large range of adjustments

from  $S_{\text{H}} = 0$  to  $S_{\text{H}} = 5$ , and our choice of the proper scaling factor sets an upper limit to  $S_{\text{H}} = 0.5$  with a best fit at  $S_{\text{H}} = 0.05$ , the value we selected for our *standard model* in Fig. 6. The scaling factor is held fixed for *all* transitions. In contrast to the results of the analyses of the solar Al I lines (Baumüller & Gehren 1996) and of the solar Mg I lines (Zhao et al. 1998) we see no trend suggesting a variation of the  $S_{\text{H}}$  with excitation energy. We note, however, that the D lines may be reproduced with quite large values of  $S_{\text{H}}$  since they do not respond to this parameter.

2. The determination of non-thermal *small-scale* broadening velocities. Granular hydrodynamics of the solar atmosphere suggest that a plane-parallel approach cannot avoid the assumption of a depth-dependent microturbulence velocity. In fact, simple tests show that — depending on the mean depth of line formation — the fit of Na line profile cores requires different values of  $\xi$ . In particular the chromospheric rise of the velocity fields is seen in the increased  $\xi$  necessary to fit the D line cores and the minimum is seen in the profile width of the  $\lambda 8190 \text{ Å}$  doublet. Except for this line the resulting fits of case (b) represented in Table 1 are forced to the same value for both lines of a doublet.
3. Van der Waals damping constants are notoriously uncertain since they depend on the description of neutral particle collisions. Holweger (1973) in his classical solar abundance analysis states that the "line broadening of strong solar Na I lines may be accounted for by van der Waals damping with interaction constants  $C_6$  increased by  $\Delta \log C_6 = 0.8$  over the value given by Unsöld's (1955) approximation". While the exact value of such a correction depends on the atmospheric model, the conclusion itself is questionable since it is based on a fit of the *equivalent widths* and not on *line profiles*. The difference is obvious from Fig. 6, where the corresponding LTE fits to the equivalent widths of the  $\lambda 8190$

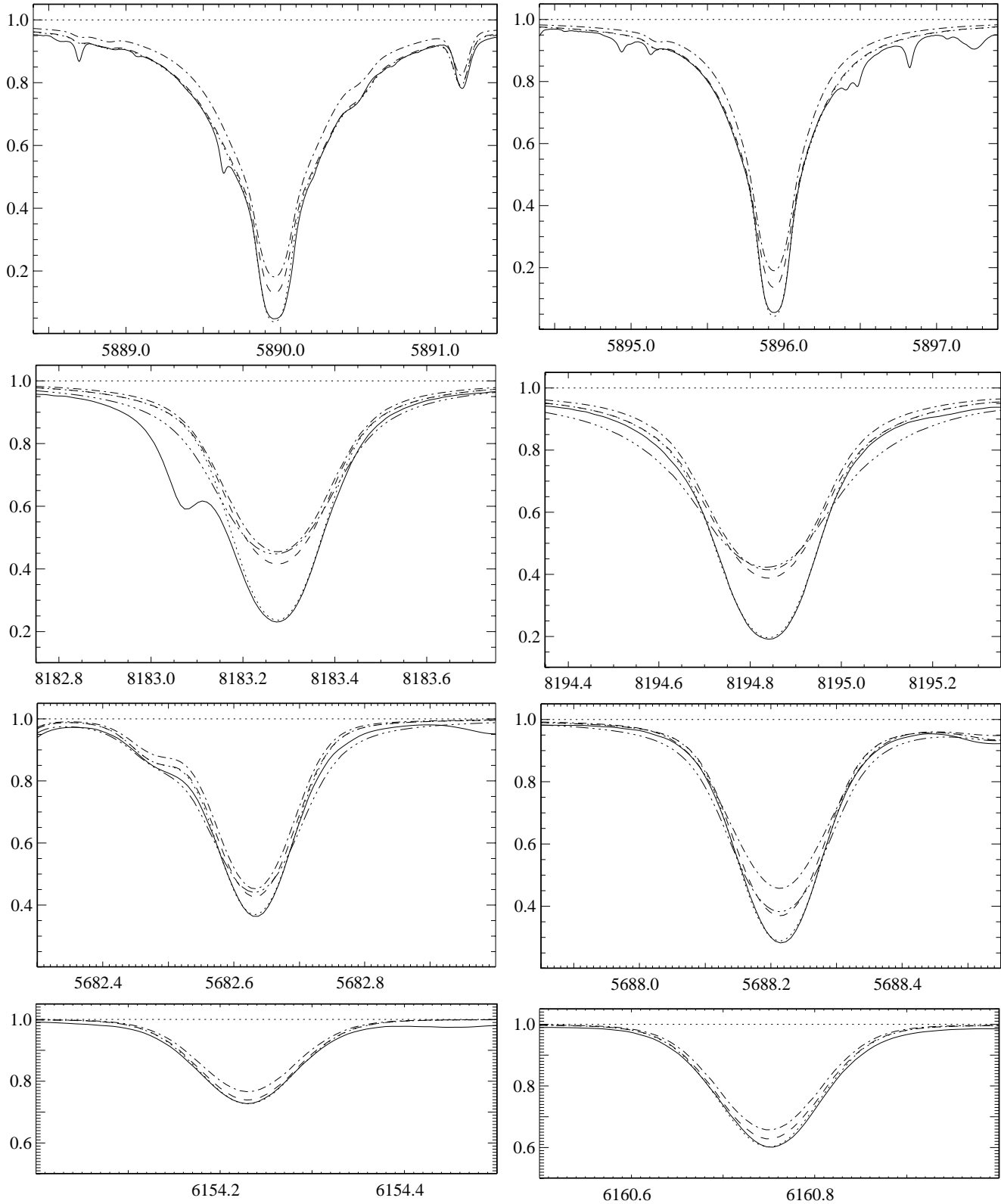


**Fig. 6.** Solar Na I flux profiles synthesized under both LTE and NLTE conditions, compared with spectra of the KPNO Solar Flux Atlas (Kurucz et al. 1984, —). All profiles are individually fitted at the line wings using van der Waals damping enhancements  $\Delta \log C_6$ , solar abundances  $\log \varepsilon_{\text{Na}, \odot}$ , appropriate microturbulence velocities  $\xi$ , and radial-tangential macroturbulent velocities  $\Xi_{\text{rt}}$ . All NLTE profiles are calculated with hydrogen collisions of  $S_{\text{H}} = 0.05$ . All plots show LTE profiles calculated with the standard atmospheric model (—) and with the model of Holweger & Müller (1974, - · -), and NLTE profiles for the standard model (· · ·). Additionally, the 8190 and 5680 doublets include LTE profiles for which the damping constant was substantially enhanced to fit the line *equivalent width* (- · · · -). (*Top row*): D lines at  $\lambda$  5890 and 5896 Å. (*Second row*):  $3p - 3d$  transitions at  $\lambda$  8193 and 8195 Å. (*Third row*):  $3p - 4d$  transitions at  $\lambda$  5683 and 5688 Å. (*Bottom row*):  $3p - 5s$  transitions at  $\lambda$  6154 and 6161 Å

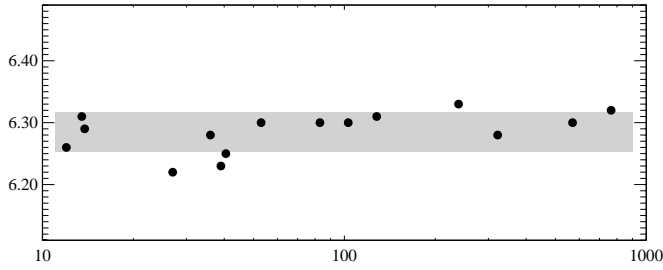


**Fig. 7.** Na I line abundances obtained from the best fit NLTE results in Table 1, plotted as a function of equivalent width. The shaded area refers to a  $1\sigma$  error excluding the  $\lambda$  8190 Å doublet (see text).

and 5680 Å doublets emphasize the failure to fit the profile wings. It is, however, possible to improve the necessary corrections for each Na I doublet by comparing the influence of damping on two lines of different strength. The results are given in Table 1 for the theoretical line-blanketed model atmosphere and they imply  $\Delta \log C_6 = 0$ .

4. The energy level splittings of Na I are small, so that all transitions to levels with  $n \geq 4$  and  $l \geq 2$  are broadened mainly by the Stark effect which we have estimated according to Hunger's (1960) approximation of the Lindholm theory. The corresponding data in Table 1 emphasize the dominant role of Stark broadening in all  $3P - nD$  transitions; for  $\lambda$  10834 Å the value had to be adjusted to fit the observed line wings with  $\log C_4 = -9.52$  instead of  $-7.52$ , for  $\lambda$  4497 Å the theoretical value was increased by a factor 10; all other data were applied as calculated.
5. The adjustment of damping parameters is most strongly coupled to the evaluation of abundances. To determine their solar photospheric value,  $\log \varepsilon_{\text{Na},\odot}$  is treated as a free parameter for each *line*. We note that the respective contributions of both  $\log \varepsilon_{\text{Na},\odot}$  and  $C_6$  (or  $C_4$ ) to the line can be disentangled using different portions of the profile. The accuracy of this procedure is between 0.05 to 0.1 for  $\log C_6$  (only for sufficiently strong lines that are sensitive to such corrections), and 0.02 for  $\Delta \log \varepsilon_{\text{Na},\odot}$ . The resulting solar abundance will be discussed below.
6. The Na I line flux profiles radiated from the top of the solar photosphere are modified by *large-scale* motions of which the rotation component can be modeled by a constant value of  $v_{\text{rot},\odot} = 1.7 \text{ km s}^{-1}$ , which accounts for the mean surface rotation of the Sun. The second component, usually termed *macroturbulence*, is best described with the radial-tangential streaming model of Gray (1977), who found that lines of different strength require corresponding adjustment of the  $\Xi_{\text{rt}}$  velocities. The optimal determination of this parameter was obtained by fitting the profiles at both line cores and the width of the shoulders between core and line wing. The variation of the resulting  $\Xi_{\text{rt}}$  roughly follows the depth-dependence of the *microturbulence*.

The parameter adjustment has been iterated to confirm and eliminate their mutual dependence as much as possible. The final results are given in Table 1 for all lines in the visible and near

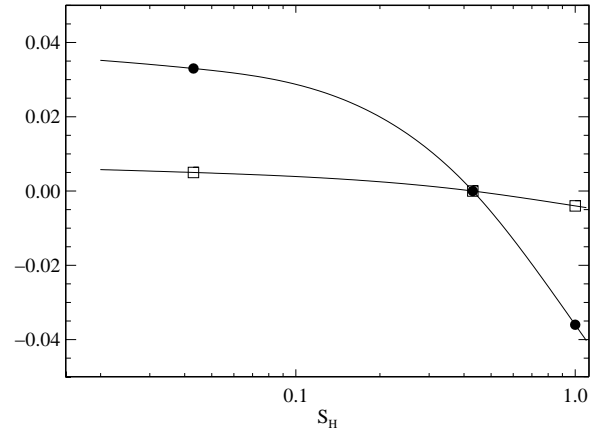


**Fig. 8.** Variation of Na I abundances  $\Delta [\text{Na}/\text{Fe}]$  determined from observed spectra with NLTE line formation calculations using different hydrogen collision scaling factors  $S_{\text{H}}$ . Results refer to the moderately metal-poor subgiant HD 69611 (open squares) and the Pop II turnoff star HD 74000 (filled circles). The zero point has been arbitrarily set at  $S_{\text{H}} = 0.5$

red spectral range that appear to be sufficiently unblended. For better comparison two cases were calculated; (a) refers to a simple solution with  $\xi = 0.9 \text{ km s}^{-1}$ , and  $\Xi_{\text{rt}} = 3.2 \text{ km s}^{-1}$  assumed for all lines. The resulting fits are improved in case (b) leaving  $\xi$  and  $\Xi_{\text{rt}}$  as free parameters for each doublet. The latter case implies some depth-dependence of the velocity fields, as is in fact observed for the Sun. However, comparison with other stars usually requires a simpler parametrization, and it is important to compare both results for the Sun in order to estimate the reliability of the stellar abundances. As a by-product of our NLTE analyses we are able to present solar Na abundances in Fig. 7. Accepting the results for all 15 lines investigated here, the best value for the mean solar abundance would be

$$\log \varepsilon_{\text{Na},\odot} = 6.284 \pm 0.035 \quad (1)$$

Closer inspection reveals that the accuracy with which the different lines are fitted with the standard NLTE model including hydrogen collisions with  $S_{\text{H}} = 0.05$  is not always perfect. If the D line NLTE abundances are used as a reference the lines in the blue yield abundances systematically lower by  $-0.05$ . This is a problem encountered also with lines of other elements in that spectral region, and it may be connected with an unidentified line haze that leads to a very uncertain continuum position. However, after removing these lines ( $\lambda\lambda$  4497, 4668, and 4751 Å) the mean abundance would be only marginally different,

$$\log \varepsilon_{\text{Na},\odot} = 6.301 \pm 0.022 \quad (2)$$

though the standard deviation would be reduced by a significant fraction. It is nearly impossible to reproduce the proper blend behaviour of  $\lambda$  8183 Å (see Fig. 6) because the blend component is unidentified; thus its present fit is more a representation of the maximum possible abundance. Moreover, the  $3p - 3d$  doublet may be marginally affected by *chromospheric* parameters that are not considered in our investigation (its mean depth

of formation being around  $\tau_c = 10^{-3}$ ). Note that all these differences are relatively small as are those obtained with respect to LTE abundances. The result of Holweger (1973) obtained with a force-fit to the damping constants of a total of 16 lines is

$$\log \varepsilon_{\text{Na}, \odot} = 6.300 \pm 0.073 \quad , \quad (3)$$

but the standard deviation is substantially larger.

The overall fit of the atomic model to the solar lines investigated here is quite satisfactory. Unlike LTE the statistical equilibrium is able to reproduce all parts of the line profiles including the line cores. The sensitivity of most lines to the scaling of hydrogen collisions is small in the solar atmosphere provided  $S_{\text{H}}$  is reduced to values below 0.5, in reasonable agreement with the results of Takeda (1995). The small differences in the adopted line parameters (cf. his Table 1) are *not* due to our respective NLTE line formation results but rather to three differences in our analysis approach,

- Takeda’s line data are based on a single doublet, unfortunately the more problematic lines at 8183 and 8194 Å ,
- the parameters entering his line formation are chosen with no further constraints. Thus e.g. his hydrogen collision scaling factor  $S_{\text{H}}$  is different for the two lines of the same doublet, and the same holds for the other parameters,
- his automatic line fit produces profiles with minimum  $\sigma^2$  but wings that are significantly deeper than observed. Such solutions cannot be accepted as realistic.

More recent investigations of the solar sodium lines are restricted to very special problems, predominantly to the reproduction of the D line profiles including their chromospheric and/or umbral contributions. Thus Bruls et al. (1992) have analyzed the response of the D lines to different solar models. Their atomic model ignores hydrogen collisions, and the influence of line-blanketing is simulated by an artificial increase in the  $\text{H}^-$  continuous opacity. Since photoionization is unimportant the latter approximation is acceptable and the  $S_{\text{H}} = 0$  option does not affect the resonance lines. Therefore their results do not add any new insight to our problem. The work of Caccin et al. (1993) discusses hydrogen collisions, but only to fit the very cores of the D lines in sunspot umbrae. This does not help to determine  $S_{\text{H}}$  factors for a complete atomic model such as the one presented here.

The available information about the role of hydrogen collisions is thus extracted from the solar spectrum and the statistical equilibrium equations can be used in the following section to obtain *spectroscopic* determinations of the sodium abundance in cool metal-poor stars.

#### 4. Sodium in metal-poor stars

Except for the D lines the analysis of *solar* sodium lines reveals a significant abundance correction with respect to LTE if abundances are determined from *line profile fits* instead of equivalent widths (see Fig. 6). Thus it is only natural to expect a more substantial effect in the atmospheres of cool stars that are reduced in metals and thus free electrons. Unlike Al with its extremely

**Table 2.** Typical abundance corrections necessary when fitting calculated NLTE equivalent widths of Na I lines in cool metal-poor stars with LTE but otherwise the same parameters. Results refer to  $[\text{Na}/\text{H}]_{\text{NLTE}} - [\text{Na}/\text{H}]_{\text{LTE}}$ . No entries are given for extremely weak lines. The representative atmospheres refer to  $\xi = 1 \text{ km s}^{-1}$  and  $[\text{Na}/\text{Fe}] = 0$

$T_{\text{eff}}$	$\log g$	[Fe/H]	Abundance corrections		
			$3s - 3p$	$3p - 3d$	$3p - 4d$
5200	4.50	0.00	-0.02	-0.11	-0.05
		-1.00	-0.08	-0.11	-0.03
		-2.00	-0.13		
		-3.00	-0.13		
		-4.00	-0.01		
5500	3.50	0.00	-0.04	-0.23	
		-1.00	-0.14	-0.14	
		-2.00	-0.32		
		-3.00	-0.30		
		-4.00	0.01		
6500	4.00	-0.00	-0.07	-0.26	
		-1.00	-0.39	-0.38	
		-2.00	-0.55		
		-3.00	-0.11		
		-4.00	-0.01		

large ground-state photoionization the statistical equilibrium of Na will depend more on the efficiency of collisions and, in the absence of free electrons, hydrogen collisions may be the only thermalizing interaction remaining. It is therefore important that the calculations in the *solar* atmospheric environment indicate that the hydrogen contribution to collisions is best described by a scaling factor  $S_{\text{H}} \ll 1$  with an upper limit corresponding to  $S_{\text{H}} \approx 0.5$ . Note that increasing  $S_{\text{H}}$  far beyond 1 will always drive the system towards LTE. The first step towards a sodium population analysis in cool metal-poor stars is therefore an investigation of the statistical equilibrium as a function of the hydrogen collision rates, parametrized as in the Sun with a scaling factor  $S_{\text{H}}$ . Typical changes due to  $S_{\text{H}}$  are reproduced in Fig. 8 for two metal-poor stars. It shows that the hydrogen collisions do not enter the results too strongly as long as they are well below  $S_{\text{H}} = 1$  with an estimated upper limit corresponding to an abundance error of  $\Delta [\text{Fe}/\text{H}] = 0.03$  dex. Together with a few more tests this confirms that our choice of  $S_{\text{H}}$  is not as important as was anticipated above. In order not to overestimate the influence of deviations from LTE a value of  $S_{\text{H}} = 0.05$  will therefore be used for most of the remaining sodium calculations in metal-poor stars.

Fig. 9 displays the typical variation of level populations with decreasing metal abundance. The corresponding decrease of the *electron collision rates* should produce the strongest effect. In fact, the departure coefficients change significantly, in particular in the metallicity range  $0 > [\text{Fe}/\text{H}] > -1$ . The departure from thermal populations is driven inwards as is the mean depth of line formation for the strongest lines. Inside  $\tau_c = 0.1$  all levels are thermalized even in the most extreme metal-poor stars. This

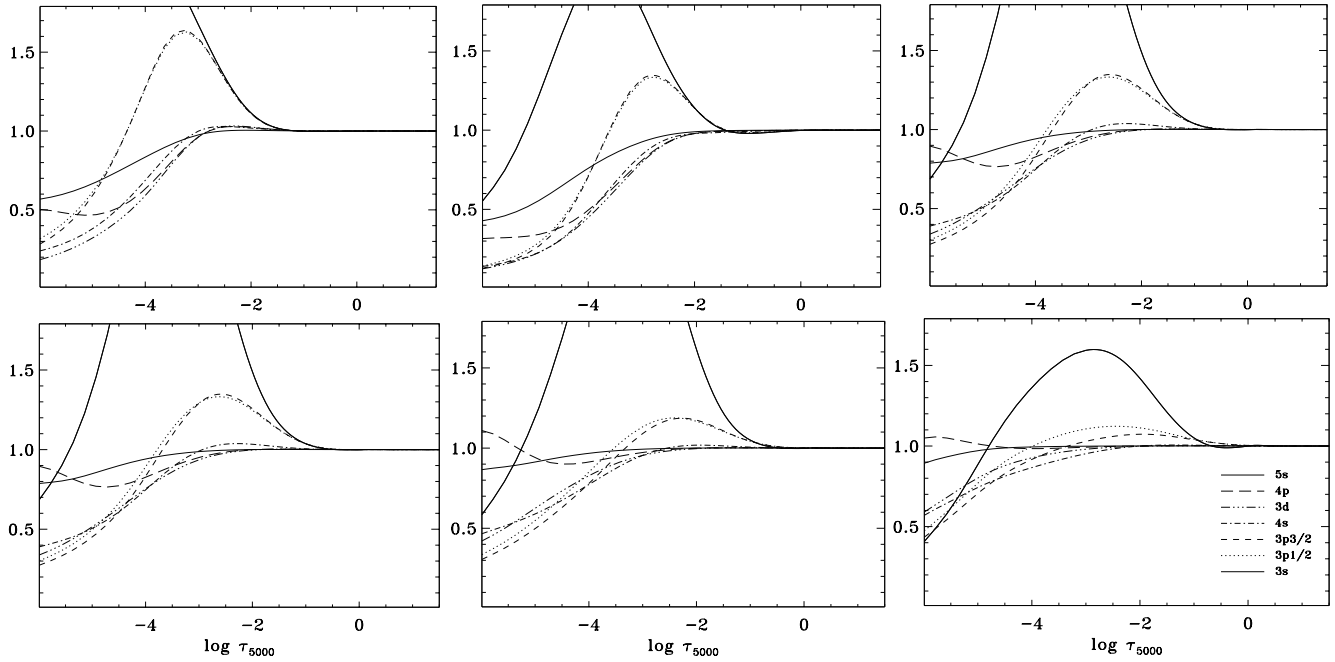


**Fig. 9.** Na I level departure coefficients  $n_k/n_k^{\text{LTE}}$  for solar-type atmospheres with  $T_{\text{eff}} = 5780$  K,  $\log g = 4.44$  but varying metal abundance. (Top row from left to right):  $[\text{Fe}/\text{H}] = 0.0, -0.5, -1.0$ . (Bottom row from left to right):  $[\text{Fe}/\text{H}] = -1.5, -2.0, -3.0$ . All NLTE calculations refer to hydrogen collisions scaled with  $S_{\text{H}} = 0.5$

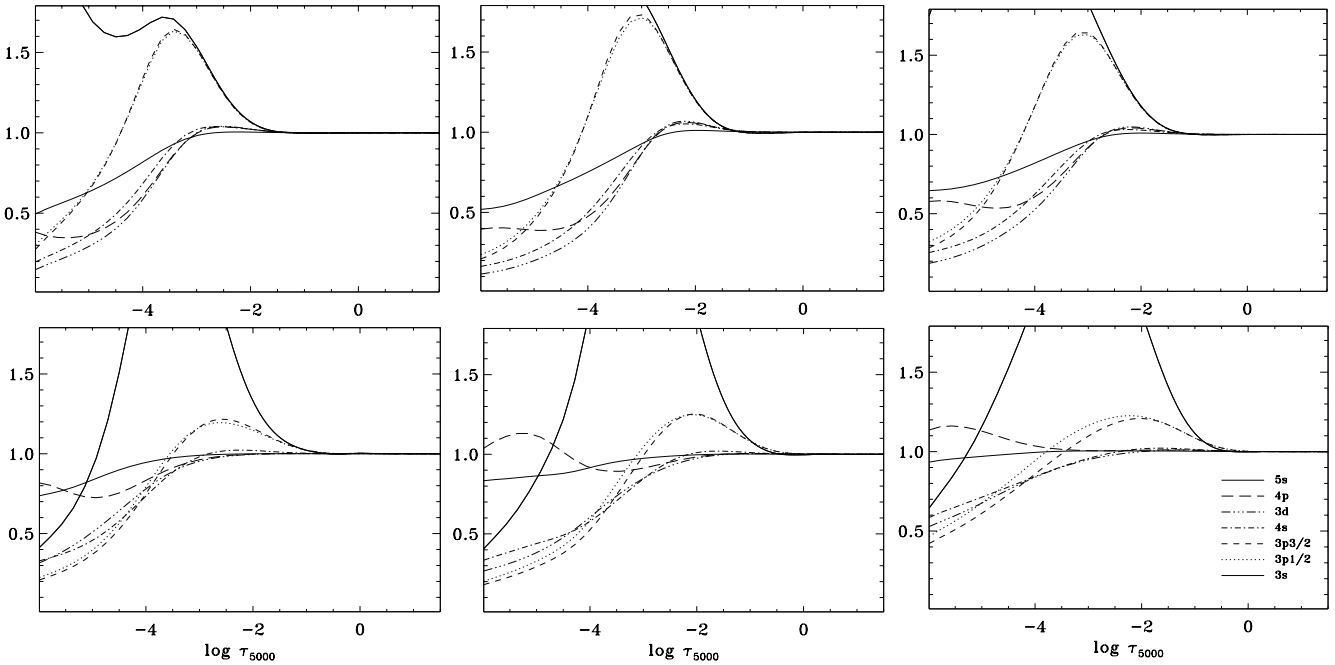


**Fig. 10.** Variation of Na I level departure coefficients for stars with different parameters. (**Top row**): typical subdwarf with  $T_{\text{eff}} = 5200$  K,  $\log g = 4.50$ ,  $[\text{Fe}/\text{H}] = 0.0$  (left); subgiant with  $T_{\text{eff}} = 5500$  K,  $\log g = 3.50$ ,  $[\text{Fe}/\text{H}] = 0.0$  (middle); hot turnoff star with  $T_{\text{eff}} = 6500$  K,  $\log g = 4.00$ ,  $[\text{Fe}/\text{H}] = 0.0$  (right). (**Bottom row**): as above, but  $[\text{Fe}/\text{H}] = -2$ .

is easily understood in terms of identifying the electron donors in moderately cool stars. After reducing the metal abundance to less than  $[\text{Fe}/\text{H}] = -2$  the remaining electrons are no longer from Mg, Si, or Fe but from hydrogen ionization; although the electron density is now substantially smaller, it is sufficient to

thermalize the Na population densities in the inner photosphere. Outside  $\tau_c = 0.01$  the relative population of the  $3p$  fine structure levels tends to become non-thermal. This effect is even stronger in slightly hotter subdwarfs (see Fig. 10), and it suggests that the forbidden electronic collision rate (assumed to be  $500 \pi a_0^2$ ) is

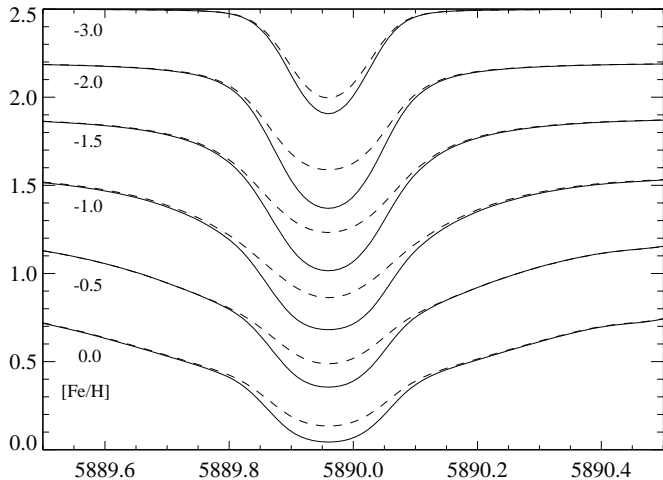


**Fig. 11.** Variation of Na I D<sub>2</sub> line profiles with metal abundance [Fe/H]. LTE profiles are dashed, NLTE profiles continuous. All other parameters are the same as in Fig. 9. Profiles for different abundances show a vertical offset of 0.3 flux units

still too low. On the other hand, the deviation of the fine structure level populations could be real; it does not, however, affect the line formation since even the D lines are formed inside  $\log \tau_c = -2$  in extremely metal-poor atmospheres. Generally, the NLTE effects are systematically stronger for the hotter models, which is in accordance with the statistical equilibrium of aluminium (see Paper I). The strongest departures from LTE are found for models with high temperature and low gravity (i.e. *turnoff* stars). The reduction of surface gravity results in a decreased efficiency of collisions by both electrons and hydrogen atoms.

From Figs. 9 and 10 it is evident that NLTE of sodium in metal-poor stars means an increased overpopulation of the ground state. Thus the formation of the D lines should be most affected and it is easy to predict that NLTE sodium abundances obtained from the resonance lines are always *smaller* than those derived from the LTE approximation. Such predictions based on model calculations follow in Table 2 below for typical solar-type dwarfs, cool subdwarfs and subgiants. As suggested by Fig. 9 the most extreme metal-poor stars will be subject only to small NLTE corrections.

#### 4.1. NLTE Line formation

In extremely metal-poor stars sodium is represented only by its resonance lines. Therefore the most important result of this analysis will be the formation of the Na D lines in stars of decreasing metal abundance. The discussion above already suggests that these lines change their appearance considerably when varying the metal abundance of a cool star from solar to typical values of halo subdwarfs. The reason for the difference with respect to LTE profiles is the decrease of collisional thermalization, and we have shown that hydrogen collisions do *not* contribute much to this process if we can trust the calibration based on the solar spectrum. The change of the  $\lambda$  5895 Å line with metal abundance [Fe/H] assuming a *solar* Na/Fe ratio is displayed in

Fig. 11. The difference between the NLTE and LTE profiles is striking, not so much at solar metallicities but mostly for metal abundances between [Fe/H] =  $-1$  and  $-2$ , where it amounts to 20% of the flux in the line cores.

The overpopulation of  $3p^2P^o$  at solar abundances *decreases* slightly in more metal-poor stars (e.g. Fig. 9) while the population of the higher excited levels varies only marginally with metal abundance. Therefore as long as the subordinate lines are sufficiently strong they will also be affected by NLTE line formation. Only in the case of metal abundances below [Fe/H]  $< -3$  will the formation of the weak D lines move into the innermost photospheric layers that are sufficiently thermalized by electron collisions, at least for effective temperatures above 5500 K. Consequently, in some of the most metal-poor subdwarfs known today, LTE profiles may be approximately valid again. The same arguments hold for the subordinate lines at slightly higher Na abundances.

#### 4.2. Sodium abundances

The D<sub>2</sub> line profiles shown in Fig. 11 make it obvious that the deep NLTE line cores in metal-deficient stars can be compensated in abundance analyses by simply increasing the Na abundance until the observed *equivalent width* is reproduced. Such results are displayed in Table 2, from which it is evident that LTE abundances can be significantly different from their NLTE counterparts, with differences reaching 0.6 dex in extreme cases.

Since in previous investigations of metal-poor stars no profile analyses were involved, the corresponding errors have not been recognized. Our present investigation starts with spectroscopic data obtained from the ESO 3.6m CASPEC, the ESO 1.5m ECHELEC, and the Calar Alto 2.2m Coudé spectrograph, however, with spectral resolutions mostly around  $R = 20000$ , which is still too low to resolve line profiles, at least for the very metal-poor stars. In addition the first observing runs with the FOCES spectrograph at the Calar Alto 2.2m and 3.5m telescopes (Pfeiffer et al. 1998) have brought a wealth of data covering the complete spectra of many subdwarfs from 4000 to 7000 Å at resolutions of  $R = 40000$  or 60000, respectively. We have added a number of these spectra to our list, and we find that the Na line profiles provide some useful constraints to the analyses.

The stellar parameters of these objects are given in Table 3. Some were taken from recent re-analyses of Fuhrmann et al. (1997), Fuhrmann (1997, private communication), and Grupp (1996). These results differ from the Axer et al. data in that their surface gravities have been rederived from the strong damping wings of neutral metal lines (and not from the Fe ionization equilibrium), now closely fitting the HIPPARCOS (1997) data. All other stars have been reanalyzed for the present investigation. For some stars the microturbulence has also been improved using an extended set of Fe lines. The abundances are all obtained from line profile fits to the resonance lines, the doublet at 5680 Å and, whenever possible, the faint doublet at 6160 Å. The external broadening function, mostly determined by the spectrograph slit, has been adjusted to fit the fainter lines in the spectrum. In the most metal-poor stars the Na abundances are

**Table 3.** Stellar parameters and sodium abundance ratios [Na/Fe]. Stellar parameters are from Fuhrmann et al. (F, 1997) and Grupp (G, 1996); all other parameters have been obtained from new analyses.  $\sigma$  refers to the standard deviation

Object	$T_{\text{eff}}$ [K]	$\log g$	[Fe/H]	$\xi$ [km/s]	Source	5889/95 Å		5682/88 Å		6154/60 Å		mean [Na/Fe] NLTE $\pm \sigma$
						LTE	NLTE	LTE	NLTE	LTE	NLTE	
HD 400	6156	4.07	-0.26	1.38	F	0.14	0.02	0.15	0.02	0.04	0.00	0.01 $\pm$ 0.02
HD 6582	5370	4.50	-0.89	1.25		0.28	0.21	0.23	0.17	0.19	0.17	0.18 $\pm$ 0.03
G245-32	6347	4.15	-1.30	1.00		-0.14	-0.46					-0.46 $\pm$ 0.01
G74-5	5742	4.60	-0.93	1.28	G	0.06	-0.04	0.00	-0.04	0.05	0.02	-0.02 $\pm$ 0.03
HD 19445	6040	4.36	-1.97	1.32	F	0.12	-0.28					-0.28 $\pm$ 0.01
G246-38	5343	4.70	-2.17	1.00	G	-0.20	-0.34					-0.34 $\pm$ 0.01
HD 22879	5790	4.40	-0.83	1.35		0.01	-0.13	-0.03	-0.10	-0.06	-0.09	-0.11 $\pm$ 0.02
G84-29	6260	4.18	-2.46	1.40	F	-0.44	-0.63					-0.63 $\pm$ 0.05
HD 45282	5270	3.17	-1.48	1.55	F	0.00	-0.33	-0.23	-0.29			-0.31 $\pm$ 0.02
HD 69611	5590	4.04	-0.68	1.45		0.08	-0.06					-0.06 $\pm$ 0.01
HD 74000	6230	4.08	-1.85	1.80		0.46	-0.09					-0.09 $\pm$ 0.02
HD 114762	5850	4.18	-0.75	1.20		0.16	0.01			0.09	0.07	0.03 $\pm$ 0.03
G64-12	6350	4.20	-2.90	1.35		-0.08	-0.57					-0.57 $\pm$ 0.07
G66-9	5980	4.55	-1.70	1.00		0.07	-0.18					-0.18
HD 140283	5810	3.71	-2.29	1.48	F	0.30	-0.24					-0.24 $\pm$ 0.05
HD 148211	5580	4.09	-0.65	1.32		-0.11	-0.23					-0.23 $\pm$ 0.02
HD 194598	6040	4.30	-1.16	1.34	F	0.17	-0.09	-0.05	-0.10	-0.06	-0.10	-0.10 $\pm$ 0.04
G212-7	5560	4.77	-1.60	1.30	G	-0.22	-0.37					-0.37 $\pm$ 0.01
HD 201891	5948	4.19	-1.05	1.15	F	0.28	0.10	0.11	0.04	0.16	0.12	0.09 $\pm$ 0.04
G25-29	5837	4.09	-0.62		F	0.19	0.06	0.15	0.06	0.11	0.07	0.06 $\pm$ 0.01
G27-45	5394	4.55	-1.38	1.00		-0.11	-0.25					-0.25 $\pm$ 0.02

obtained exclusively from the D lines. The results are reproduced in Table 3, where both the NLTE profile fit abundances and the LTE abundances yielding the same equivalent widths are listed for comparison. One of the most striking results is the change between LTE and NLTE abundances corresponding to a factor 3.5 in the very metal-poor subgiant HD 140283. This is representative for similarly metal-poor stars. Thus, all stars with [Fe/H] below  $-1.4$  show *subsolar* NLTE abundance ratios [Na/Fe], whereas their LTE abundances would be substantially above solar.

Considering only LTE abundances based on the fit of equivalent widths it is conspicuous how the abundances determined from the D lines and the 5680 Å or the 6160 Å doublets differ. Note that in most cases these differences are well above the observational errors. Alternatively, the NLTE abundances based on profile fits produce a satisfactory standard deviation when including lines from all doublets and they compare favourably with the *solar* abundance errors. Moreover, the standard deviation of the NLTE results is between a factor 5 to 2 lower than for the LTE data. This result is perhaps the most important because it shows that with high S/N spectra of sufficient spectral resolution ( $R = 40000$  or higher) it is possible to reproduce line profiles with a very high accuracy. A few profile fits for the subgiant HD 45282 are shown in Fig. 12. They are representative for the *average* fit quality obtained for the  $R = 40000$  FOCES spectra.

Table 3 displays the Na abundances of all stars investigated. The NLTE mean abundance data are reproduced together with the nominal standard deviation of a single line, i.e. the error of

the mean would be correspondingly smaller. Systematic errors depend on the validity of the plane-parallel model atmosphere concept. It implies that  $T_{\text{eff}}$  and  $\log g$  can be uniquely determined, and that hydrodynamic motions can be modeled with the micro- and macroturbulence velocities,  $\xi$  and  $\Xi$ . The non-thermal velocity parameters, in particular, reflect all the uncertainties of the simple model atmosphere approach. Therefore in some stars the faint 6160 Å lines seem to require a slightly different *external* broadening parameter than do the D lines. It will be necessary to analyze some of the line profiles with higher resolution, but even at  $R = 60000$  there does not seem to be any alternative to the introduction of a depth-dependent turbulent velocity. Most interestingly, the obvious requirements concern more the external broadening parameters than the microturbulence, and therefore the abundance results should not be very sensitive to this problem.

However,  $T_{\text{eff}}$  and  $\log g$  are important and the accuracy of their determination enters the final NLTE abundances as much as in the LTE data. Since the determinations of  $T_{\text{eff}}$  and  $\log g$  are still mutually dependent, we estimate the *systematic* errors to be of the order of 0.05 dex for the best spectra. As long as model atmospheres are used *differentially* both the analysis of the Balmer line wings and that of the damping wings of the strong Mg I and Fe I lines are among the most reliable methods used in spectrum synthesis, i.e. they are much better defined than any synthetic colours. This has been demonstrated recently by Fuhrmann et al. (1997) and Fuhrmann (1998) who found that the surface gravity determined from the iron ionization equilibrium is different from that obtained using HIPPARCOS parallaxes in

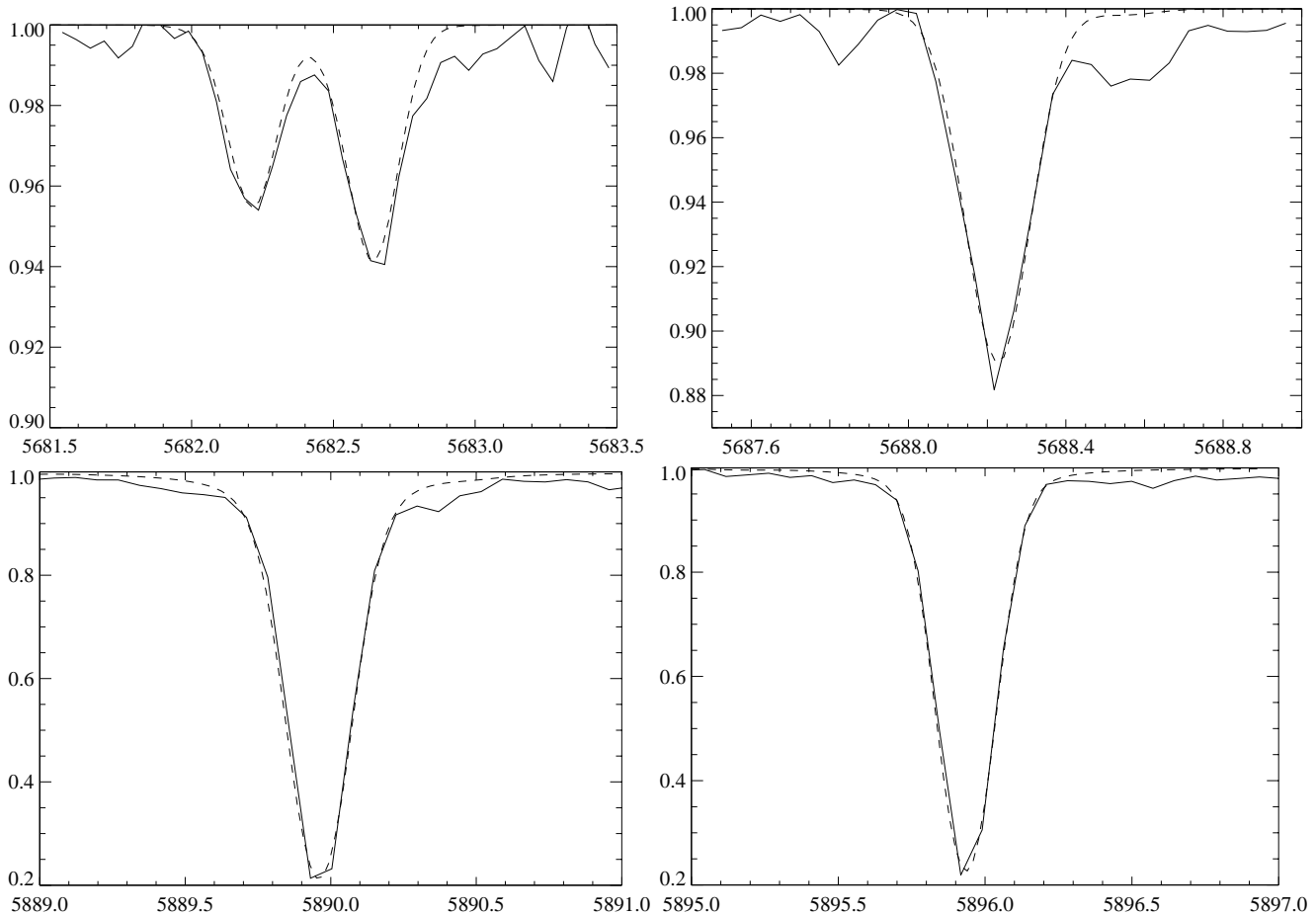


**Fig. 12.** Line profile fits for HD 45282. NLTE profiles are dashed. Observed profiles are from FOCES spectra obtained with  $R = 40000$  resolution

most of the metal-poor stars. Consequently, for a number of stars for which new spectra were obtained with the FOCES spectrograph (Pfeiffer et al. 1998) new stellar parameters have been determined with surface gravities conforming to the HIPPARCOS results (1997).  $[\text{Fe}/\text{H}]$  has been determined only from Fe II lines; this moved the metal abundance scale towards values substantially more metal-rich than previously accepted and the  $[\text{Na}/\text{Fe}]$  data tend towards correspondingly smaller results. The main effect, however, is due to the adjustment of the surface gravities dictated by the HIPPARCOS observations.

Carlsson et al. (1994) have investigated the formation of the Li I resonance lines under NLTE conditions in cool stars. Although Li and Na have similar atomic structures, photoionization from the 3s and 3p levels of Na I is less important than that of the corresponding Li I levels. Consequently, photon suction plays the dominant role in Na I whereas the Li I population is apparently more sensitive to overionization. Our Na I abundance corrections are *all* negative and they are particularly important for metal-poor stars. We note that only for the most metal-poor subdwarfs ( $[\text{Fe}/\text{H}] = -3$ ) the absolute abundances of Li and Na become comparable, and in that range the abundance corrections of the Na and Li resonance lines are very similar.

## 5. Discussion

The variation of  $[\text{Na}/\text{Fe}]$  with the stellar mean metal abundance  $[\text{Fe}/\text{H}]$  contains information about the chemical evolution of the Galaxy. Previous data are all based on LTE and Fig. 1 seems to advocate the existence of an essentially *solar* sodium abundance ratio. These results are in rough agreement with our results assuming LTE and *ignoring line profiles*. In the data of McWilliam et al. (1995) there is an apparent overabundance of Na with respect to Fe in some of the most metal-poor stars, but that could also be interpreted as an intrinsic scatter around  $[\text{Na}/\text{Fe}] = 0$ . It is, however, obvious that the standard Timmes et al. chemical evolution model differs significantly from the LTE abundances. This model is based on some of the most recent stellar evolution calculations (Woosley & Weaver 1995), and for Na I it represents mainly the results of carbon and neon burning in the very first stellar generations.

As already discussed above, our NLTE  $[\text{Na}/\text{Fe}]$  abundance ratios differ from the LTE results; at low metallicities all Na abundance ratios now become *subsolar*. For  $[\text{Fe}/\text{H}] < -3$  we have no data since our object list was restricted to subdwarfs and subgiants. Note, that G64-12 on our new Fe II abundance scale is moved to  $[\text{Fe}/\text{H}] = -2.9$ . All abundance results are collected in

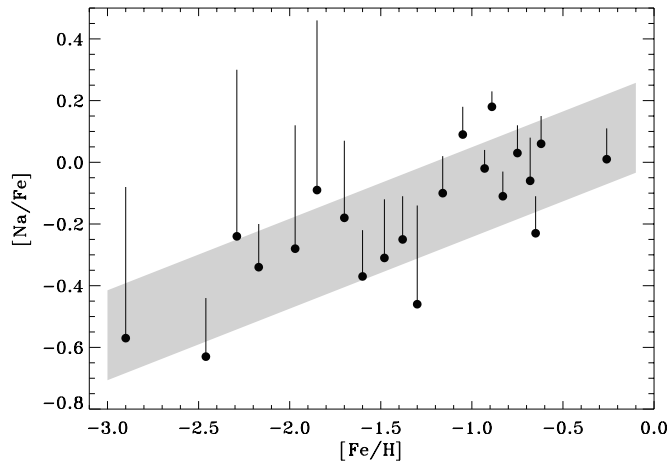


**Fig. 13.** NLTE sodium abundances; vertical bars denote the individual corrections applying to an LTE analysis (cf. Table 3). The shaded area refers to a mean relation with a  $1\sigma$  error

Fig. 13 which looks quite different from Fig. 1. The necessary corrections for NLTE are large, in particular for very metal-poor *turnoff* stars ( $T_{\text{eff}} > 6000\text{K}$ ). The admittedly very sparse data allow one to conclude that there is a steady decline in the  $[\text{Na}/\text{Fe}]$  vs.  $[\text{Fe}/\text{H}]$  distribution from solar abundances down to  $[\text{Fe}/\text{H}] \approx -3$ . Since the scatter of the  $[\text{Na}/\text{Fe}]$  data around the mean fit is large compared with the observational errors of the analyses, the abundance scatter could be real.

Since the two most metal-poor stars in the sample, G64-12 and G84-29, do not seem to be peculiar, the new results are in even stronger contradiction to the Timmes et al. (1995) calculations than are the McWilliam et al. LTE data. These two extremely metal-poor turnoff stars are definitely *underabundant* in Na by a large amount.

**Acknowledgements.** This research was supported by the Deutsche Forschungsgemeinschaft under grants Ge 490/10-1 and -2; the FOCES spectrograph would have not been built without grants 05 5MU414(8) and 05 2MU114(7) from the German ministry of science and technology (BMFT). We thank Johannes Reetz for his strong support with the spectrum synthesis. Some of the spectra have been kindly made available by Klaus Fuhrmann

## References

- Athay R.G., Canfield R.C. 1969, ApJ 156, 695  
 Auer L.H., Heasley J.N., 1976, ApJ 205, 165  
 Axer M., Fuhrmann K., Gehren T. 1994, A&A 291, 895  
 Baumüller D., Gehren T. 1996 A&A 307, 961 (Paper I)  
 Baumüller D., Gehren T. 1997 A&A 325, 1088 (Paper II)  
 Bessell M.S., Norris J. 1984, ApJ 285, 622  
 Bruls J.H.M.J., Rutten R.J., Shchukina N.G., 1992, A&A 265, 237  
 Butler K. 1993, unpublished  
 Butler K., Giddings J. 1985, Newsletter on Analysis of Astronomical Spectra No. 9, University of London  
 Caccin B., Gomez M.T., Roberti G. 1980, A&A 92, 63  
 Caccin B., Gomez M.T., Severino G. 1993, A&A 276, 219  
 Carlsson M., Rutten R.J., Bruls J.H.M.J., Shchukina N.G. 1994, A&A 288, 860  
 Cunto W., Mendoza C., Ochsenbein F., Zeippen C.J. 1993, A&A 275, L5  
 Drawin H.W. 1968, Z. Physik 211, 404  
 Edvardsson B., Anderson J., Gustafsson B., Lambert D.L., Nissen P.E., Tomkin J. 1993, A&A 275, 101  
 Fuhrmann K. 1998, A&A submitted  
 Fuhrmann K., Pfeiffer M., Reetz J., Gehren T. 1997, A&A 323, 909  
 Gehren T. 1975, A&A 38, 289  
 Giddings J.R. 1981, Ph.D. thesis, University of London  
 Gratton R.G., Sneden C. 1987, A&A 178, 179  
 Gratton R.G., Sneden C. 1988, A&A 204, 193  
 Gray D.F. 1977, ApJ 218, 530  
 Green L.C., Rush P.P., Chandler C.D. 1957, ApJS 26, 37  
 Grupp F. 1996, Diploma thesis, Universität München  
 HIPPARCOS Catalogue 1997, electronic version, CDS, Strasbourg  
 Holweger H. 1973, A&A 10, 128  
 Holweger H. 1979, in *Les Elements et leurs Isotopes dans l'Univers*, 22<sup>nd</sup> Liège Symp., Liège, p. 117  
 Holweger H., Müller E.A. 1974, Sol. Phys. 39, 19  
 Hunger K. 1960, Z. Astrophys. 49, 131  
 Kaulakys B. 1985, J. Phys. B. 18, L167  
 Kaulakys B. 1986, Sov. Phys. JETP 64, 229  
 Kurucz R.L. 1992, Rev. Mex. Astron. Astrof. 23, 181  
 Kurucz R.L., Furenlid I., Brault J., Testerman L. 1984, Solar Flux Atlas from 296 to 1300 nm, Kitt Peak National Solar Observatory  
 Lambert D.L. 1993, Phys. Scripta T47, 186  
 Martin W.C., Zalubas R. 1981, J. Phys. Chem. Rev. Data, 153  
 Mashonkina L.I., Sakhbullin N.A., Shimanskii V.V. 1993, Astron. Rep. 37, 192  
 Mashonkina L., Shimanskii V., Ivanova D., Sakhbullin N. 1998, submitted to A&A  
 McWilliam A., Preston G., Sneden C., Searle L. 1995, AJ 109, 2736  
 Peterson R.C. 1981, ApJ 244, 989  
 Pfeiffer M., Frank C., Baumüller D., Fuhrmann K., Gehren T. 1998, A&A in press  
 Sampson D.H., Zhang H.L. 1992, Phys. Rev. A 45, 1556  
 Steenbock W., Holweger H. 1984, A&A 130, 319  
 Stürenberg S., Holweger H. 1990, A&A 237, 125  
 Takeda Y. 1995, PASJ 47, 463  
 Timmes F.X., Woosley S.E., Weaver T.A. 1995, ApJS 98, 617  
 Unsöld A. 1955, Physik der Sternatmosphären, Springer-Verlag, Berlin-Heidelberg  
 van Regemorter H. 1962, ApJ 136, 906  
 Woosley S.E., Weaver T.A. 1995, ApJS 101, 181  
 Zhao G., Butler K., Gehren T. 1998, A&A in press